Magn Reson Med Sci 2019; 18; 233–237
doi:10.2463/mrms.tn.2018-0068
Published Online: December 6, 2018

TECHNICAL NOTE

Improved Visualization of Middle Ear Cholesteatoma with Computed Diffusion-weighted Imaging

Koji Yamashita[1*], Akio Hiwatashi[1], Osamu Togao[1], Kazufumi Kikuchi[1], Yamato Shimomiya[2], Ryotaro Kamei[1], Daichi Momosaka[1], Nozomu Matsumoto[3], Kouji Kobayashi[4], Atsushi Takemura[5], Thomas Christian Kwee[6], Taro Takahara[7], and Hiroshi Honda[1]

Computed DWI (cDWI) is a mathematical technique that calculates arbitrary higher *b* value images from at least two different lower *b* values . In addition, the removal of high intensity noise with image processing on cDWI could improve cholesteatoma-background contrast-to-noise ratio (CNR). In the present study, noise reduction was performed by the cut-off values of apparent diffusion coefficient (ADC) less than 0 and 0.4×10^{-3} s/mm^2. The cholesteatoma to non-cholesteatoma CNR was increased using a noise reduction algorithm for clinical setting.

Keywords: *cholesteatoma, diffusion weighted imaging, magnetic resonance imaging, middle ear, signal-to-noise ratio*

Introduction

Diffusion-weighted MR imaging (DWI) is the most widely used imaging technique for the detection of middle ear cholesteatoma.[1–8] Turbo spin echo (TSE) DWI could reduce geometric distortions compared to echo-planar imaging (EPI) based acquisitions, and shows promise for the application in the middle ear region.[3,4] On the other hand, it is known that the TSE–DWI sequence as well as higher *b* value (>1000 s/mm^2) suffer from inherently lower signal-to-noise ratio (SNR).[9,10]

Computed DWI (cDWI) is a mathematical technique that calculates arbitrary higher *b* value images from at least two different lower *b* values. This may avoid eddy current distortions while keeping higher SNR.[11,12] Recently, the utility of cDWI for prostate cancer or hepatic metastases detection using has been reported in the literatures.[11,13–15] In contrast, the application of cDWI for middle ear diseases has not been explored yet. One potential drawback of cDWI is that voxels less than 0 s/mm^2 in ADC are practically present using voxel-by-voxel based calculation, which could reduce diagnostic quality. Removal of high intensity noise with image processing on cDWI could improve cholesteatoma to non-cholesteatoma contrast-to-noise ratio (CNR). Our purpose was to evaluate whether cDWI with a noise reduction algorithm increases CNR compare to that without noise reduction in middle ear cholesteatoma.

Materials and Methods

Case selection

This retrospective study was approved by Kyushu University Institutional Review Board for Clinical Research, and the requirement for written informed consent was waived. Consecutive patients diagnosed with suspected cholesteatoma who underwent preoperative MR imaging between October 2014 and August 2016 were eligible for inclusion. Two subjects were excluded from the study due to motion artifacts on DWI. Each patient underwent preoperative MRI on the day before surgery. All of the patients were confirmed the diagnosis of cholesteatoma at surgery.

Image acquisition

All images were obtained using a 3T MR imaging unit (Ingenia CX, Philips Medical Systems, Best, The Netherlands) with a 15-channel head array receiving coil for sensitivity encoding (SENSE) parallel imaging. The single-shot TSE–DWI scanning parameters were as follows: TR/TE = 4200/84 ms; flip

[1]Department of Clinical Radiology, Graduate School of Medical Sciences, Kyushu University, 3-1-1 Maidashi, Higashi-ku, Fukuoka, Fukuoka 812-8582, Japan
[2]Division of Marketing, Department of Clinical Application Development, Ziosoft, Inc., Tokyo, Japan
[3]Department of Otorhinolaryngology, Graduate School of Medical Sciences, Kyushu University, Fukuoka, Japan
[4]Department of Medical Technology, Kyushu University Hospital, Fukuoka, Japan
[5]Philips Healthcare, Best, The Netherlands
[6]Department of Radiology, Nuclear Medicine and Molecular Imaging, University Medical Center Groningen, Groningen, The Netherlands
[7]Department of Biomedical Engineering, Tokai University, School of Engineering, Kanagawa, Japan
*Corresponding author, Phone: +81-92-642-5695, Fax: +81-92-642-5708, E-mail: yamakou@radiol.med.kyushu-u.ac.jp

Received: March 21, 2018 | Accepted: October 24, 2018

angle = 90°; echo train length = 46; refocusing control angle = 100°; b value = 0, 400 s/mm^2; motion probing gradient = 3 orthogonal directions; effective diffusion time = 13.1 ms (diffusion gradient separation = 15.5 ms; diffusion gradient pulse duration = 7.1 ms); SENSE factor = 2; slice thickness/gap = 1.5/0 mm; slices = 18; acquisition matrix = 152 × 154; FOV = 230 mm; number of signal averages = 5. The total acquisition time was 2 m 48 s. DWIs with 1.5 mm isotropic voxels were generated for evaluation.

Image evaluation

Maps of ADC were calculated using the following formula: $\ln(S/S_0) = -b \times \mathrm{ADC}$, where S_0 and S are the signal intensities for b values are 0 and 400 s/mm^2, respectively, and b itself is 400 s/mm^2. cDWI (b = 800 s/mm^2) was generated from two b values of 0 and 400 s/mm^2 by voxelwise fitting on a 3D workstation (Ziostation2, Ziosoft Inc., Tokyo, Japan) by using the following formula:

$$S(b_{800}) = S(0)e^{-b_{800} \times \mathrm{ADC}}$$

It is well-known that ADC value displays positive value mathematically. In addition, previous reports have indicated that lower limit of ADC value in the musculoskeletal[16] or endometrial malignant tumor[17] was approximately 0.4 × 10^{-3} mm^2/s. Therefore, noise reduction was performed with the cut-off values of ADC < 0 (ADC_0) and 0.4 × 10^{-3} mm^2/s ($\mathrm{ADC}_{0.4}$) on the 3D workstation (Ziostation2). ROIs were manually placed by a neuroradiologist (KY with 16 years of experience) on the cholesteatoma, soft tissue adjacent to the cholesteatoma (non-cholesteatoma), and the contralateral cerebellum, respectively (Fig. 1). Careful attention was paid to avoid contamination of air for ROI positioning. The Ziostation2 software was used to draw the ROIs. The same ROIs were set up for ADC_0, $\mathrm{ADC}_{0.4}$, and the control (without noise reduction algorithm).

Image analysis

The CNR was calculated by using the following formula:

$$\mathrm{CNR} = (\mathrm{SI}_{\text{cholesteatoma}} - \mathrm{SI}_{\text{non-cholesteatoma}})/\mathrm{SD}_{\text{non-cholesteatoma}},$$

where $\mathrm{SD}_{\text{non-cholesteatoma}}$ is the standard deviation of the signal intensity (SI) within the ROI. The noise distribution is not homogeneous in parallel imaging, so it is good to estimate noise in close proximity to the site of SI measurement.[18,19] In addition, the signal intensity ratio (rSI) of cholesteatoma to the contralateral cerebellum was calculated. The differences in the CNR and rSI were compared between ADC_0, $\mathrm{ADC}_{0.4}$, and the control using one-way ANOVA followed by the Bonferroni correction for multiple comparison. Statistical analyses were performed using Graphpad Prism 5 (GraphPad Software Inc., San Diego, CA, USA). In the statistical analysis, the level of significance was set at $P < 0.05$.

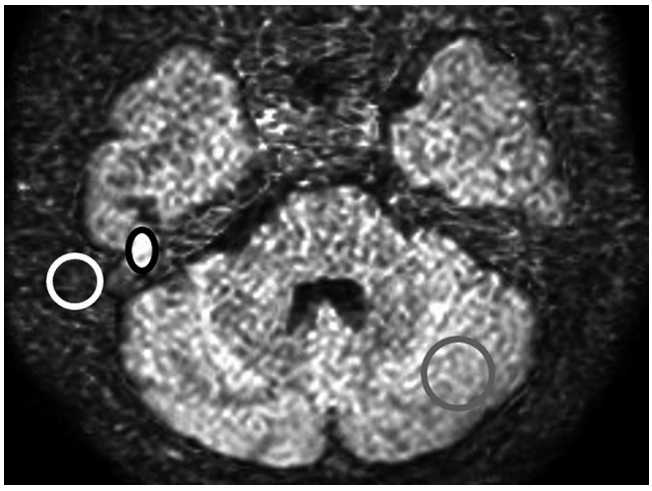

Fig. 1 Example of ROI placement on turbo spin echo-diffusion-weighted MR imaging (TSE–DWI). ROIs were placed on the probable cholesteatoma location (black circle), soft tissue adjacent to the cholesteatoma (non-cholesteatoma; white circle), and the contralateral cerebellum (grey circle).

Results

A total of 25 patients (M: F =14:11; median age = 51 years; range, 14–78 years) with unilateral cholesteatoma were finally analyzed.

The average post-processing time was a few seconds.

All values are expressed as mean ± SD. Figure 2a shows the CNR of $\mathrm{ADC}_{0.4}$ could be increased thanks to the noise reduction algorithm in the vast majority of subjects. The CNR of $\mathrm{ADC}_{0.4}$ (7.24 ± 1.70) was significantly higher than those of the control (6.09 ± 1.80; P = 0.0023) and ADC_0 (5.85 ± 1.20; P = 0.0021). We observed no significant differences between the CNR of the control and that of ADC_0.

Figure 3 indicates that the rSI of $\mathrm{ADC}_{0.4}$ (1.32 ± 0.31) tends to exhibit higher value compared with that of the control (1.14 ± 0.25; P = 0.08) or ADC_0 (1.15 ± 0.26; P = 0.10), although no significant differences were found.

Figures 4 and 5 show representative cases.

Discussion

In the present study, we evaluated whether cDWI with a noise reduction algorithm would improve cholesteatoma to non-cholesteatoma CNR compared to cDWI without noise reduction algorithm. Our result show that the CNR could be increased for $\mathrm{ADC}_{0.4}$ compared to the control. The noise reduction with the cut-off value of 0.4 × 10^{-3} mm^2/s is reasonable for clinical setting because it is assumed that the lower limit of ADC value in tumor tissue is approximately 0.4 × 10^{-3} mm^2/s.[16,17] Previous reports have shown that the improvement of diagnostic accuracy results from increasing suppression of the background signal.[11,14] In addition, the average post-processing time was only a few seconds.

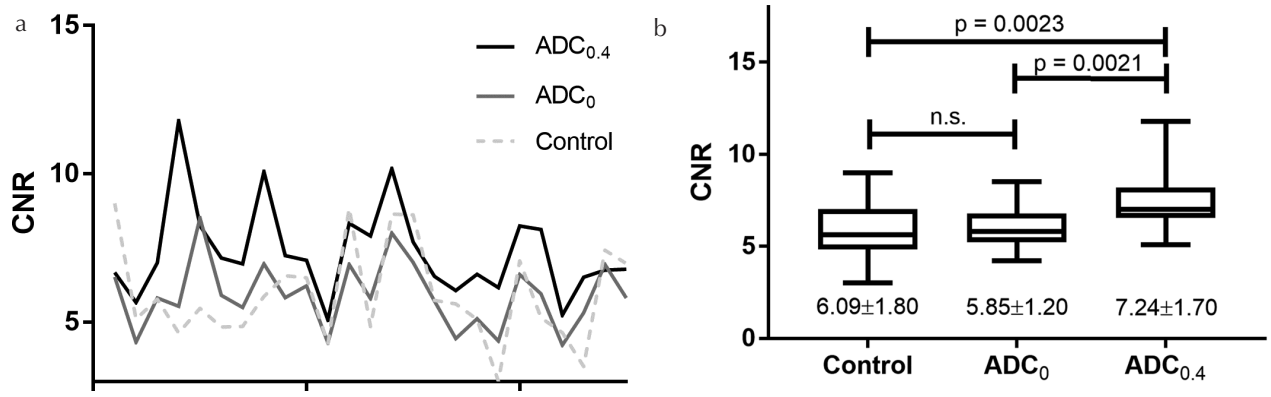

Fig. 2 Comparison of CNR among the control, ADC_0, and $ADC_{0.4}$. (**a**) The line chart showing the CNR of $ADC_{0.4}$ could be increased thanks to the noise reduction algorithm in the vast majority of subjects. (**b**) The boxplots reveal that the CNR of $ADC_{0.4}$ are significantly higher than those of the control and ADC_0. No significant differences are found between the CNR of the control and that of ADC_0. ADC, apparent diffusion coefficient; CNR, contrast-to-noise ratio.

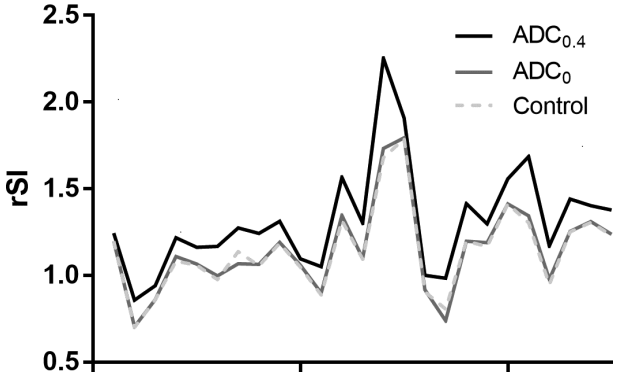

Fig. 3 Line chart of rSI among the control, ADC_0, and $ADC_{0.4}$. The rSI of $ADC_{0.4}$ tends to exhibit higher value compared with that of the control or ADC_0, although no significant differences are found. ADC, apparent diffusion coefficient; rSI, signal intensity ratio.

Therefore, cDWI with noise reduction algorithm is easily feasible in routine clinical practice.

The rSI of $ADC_{0.4}$ tends to exhibit higher value compared with that of the control and ADC_0. It is not surprising that cDWI with noise reduction algorithm may be useful to distinguish cholesteatoma from adjacent granulation or fibrous tissue, whereas our study found that most subjects had only small amount of granulation or fibrous tissue around their cholesteatoma. Further experiments would be necessary in the near future.

The utility of cholesteatoma diagnosis using a non-EPI DWI technique has been reported in the literature.[3,4,20] TSE–DWI is known to reduce curvilinear artifacts at the air–bone interface of the temporal bone because of its minimal image distortion compared with EPI-based DWI, and useful for the detection of even small cholesteatomas. DWI with high *b* value is necessary for the cholesteatoma detection, while an additional number of excitations is required to compensate for the SNR reduction, which tends to prolong the scanning time. Another drawback includes motion artifact due to prolongation of scanning time. In the present study, higher *b* value images (cDWI) were generated from the two different lower *b* values while maintaining adequate CNR. We hypothesized that the noise reduction algorithm was useful because of increase of high intensity noise (or artifact) due to the air–bone interface in the temporal bone region. Consequently, the usefulness of the noise reduction algorithm was proven in this study.

The *b* value of 800 s/mm^2 was computationally generated in the present study. The optimum *b* value has not yet been determined for the head and neck region. Although we should evaluate other *b* values, *b* values between 800 and 1000 s/mm^2 have been most commonly used.[1–8,14,20] In addition, the *b* value itself is not an important factor[21] because ADC values strongly depends on the effective diffusion time.[22] Thus, we believe that the effect of different *b* values distorted our results only minimally.

Our study has some limitations. First, the originally acquired DWI dataset (b = 800 s/mm^2) was not evaluated. The effective diffusion time affects ADC value, which may reflect the restriction of water diffusion.[22] Andica et al.[22] reported that the different effective diffusion time resulted in the different ADC value of the epidermoid cysts. In our study, the diagnosis of cholesteatoma was confirmed during surgery in all cases. However, it should be taken into account that there is a difference of the diffusion time between the originally acquired and computed DWI. Second, the CNR of TSE–DWI was not compared with that of EPI-based DWI. Third, the optimum cut-off value was not evaluated in the present study. The voxels less than 0.4×10^{-3} mm^2/s in ADC are not practically present. However, excessive noise reduction may cause inhomogeneous intensity in $ADC_{0.4}$ images. The determination of the optimum cut-off value will be our next step and that is one of the current limitations.

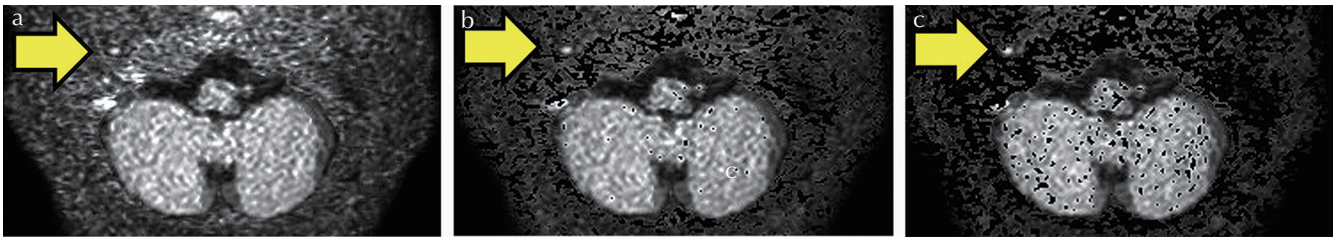

Fig. 4 A 69-year-old man with right middle ear cholesteatoma. The control image on TSE–DWI (**a**) shows the cholesteatoma as mild high intensity in the epitympanum. The ADC_0 (**b**) and $ADC_{0.4}$ (**c**) images demonstrate the lesions with conspicuous high intensity in both images. ADC, apparent diffusion coefficient; TSE–DWI, turbo spin echo-diffusion-weighted MR imaging.

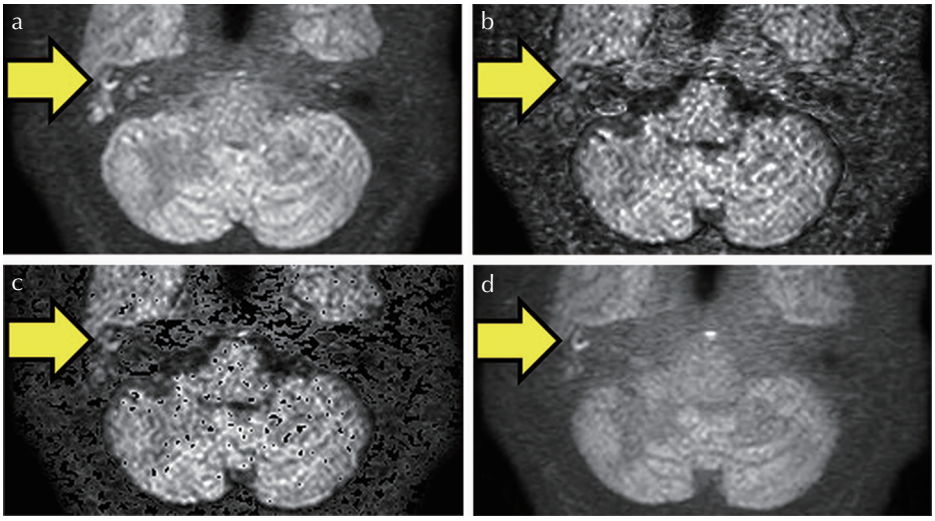

Fig. 5 A 45-year-old man with right middle ear cholesteatoma. The TSE–DWI (b = 400 s/mm^2; effective diffusion time = 13.1 ms; number of signal averages = 5; (**a**) shows the cholesteatoma with dorsal chronic inflammatory change. The control (**b**) and $ADC_{0.4}$ (**c**) images demonstrate the marked reduction of the SI of the non-cholesteatomous lesion in both images. The corresponding originally acquired TSE–DWI (b = 800 s/mm^2; effective diffusion time = 14.7 ms; number of signal averages = 10; (**d**) is indicated as a reference. ADC, apparent diffusion coefficient; SI, signal intensity; TSE–DWI, turbo spin echo-diffusion-weighted MR imaging.

Conclusion

The cholesteatoma to non-cholesteatoma CNR was increased using a noise reduction algorithm for clinical setting.

Conflicts of Interest

Yamato Shimomiya is an employee of Ziosoft, Atsushi Takemura is an employee of Philips. The remaining authors declare that they have no conflict of interest.

References

1. Aikele P, Kittner T, Offergeld C, Kaftan H, Hüttenbrink KB, Laniado M. Diffusion-weighted MR imaging of cholesteatoma in pediatric and adult patients who have undergone middle ear surgery. AJR Am J Roentgenol 2003; 181:261–265.
2. De Foer B, Vercruysse JP, Bernaerts A, et al. The value of single-shot turbo spin-echo diffusion-weighted MR imaging in the detection of middle ear cholesteatoma. Neuroradiology 2007; 49:841–848.
3. De Foer B, Vercruysse JP, Bernaerts A, et al. Middle ear cholesteatoma: non-echo-planar diffusion-weighted MR imaging versus delayed gadolinium-enhanced T1-weighted MR imaging–value in detection. Radiology 2010; 255:866–872.
4. De Foer B, Vercruysse JP, Pilet B, et al. Single-shot, turbo spin-echo, diffusion-weighted imaging versus spin-echo-planar, diffusion-weighted imaging in the detection of acquired middle ear cholesteatoma. AJNR Am J Neuroradiol 2006; 27:1480–1482.
5. Dubrulle F, Souillard R, Chechin D, Vaneecloo FM, Desaulty A, Vincent C. Diffusion-weighted MR imaging sequence in the detection of postoperative recurrent cholesteatoma. Radiology 2006; 238:604–610.
6. Lehmann P, Saliou G, Brochart C, et al. 3T MR imaging of postoperative recurrent middle ear cholesteatomas: value of periodically rotated overlapping parallel lines with enhanced reconstruction diffusion-weighted MR imaging. AJNR Am J Neuroradiol 2009; 30:423–427.
7. Vercruysse JP, De Foer B, Pouillon M, Somers T, Casselman J, Offeciers E. The value of diffusion-weighted MR imaging in the diagnosis of primary acquired and residual cholesteatoma: a surgical verified study of 100 patients. Eur Radiol 2006; 16:1461–1467.
8. Yamashita K, Yoshiura T, Hiwatashi A, et al. Detection of middle ear cholesteatoma by diffusion-weighted MR imaging: multishot echo-planar imaging compared with single-shot echo-planar imaging. AJNR Am J Neuroradiol 2011; 32:1915–1918.
9. Yoshida T, Urikura A, Shirata K, Nakaya Y, Terashima S, Hosokawa Y. Image quality assessment of single-shot turbo spin echo diffusion-weighted imaging with parallel

imaging technique: a phantom study. Br J Radiol 2016; 89:20160512.
10. Jones DK, Horsfield MA, Simmons A. Optimal strategies for measuring diffusion in anisotropic systems by magnetic resonance imaging. Magn Reson Med 1999; 42:515–525.
11. Blackledge MD, Leach MO, Collins DJ, Koh DM. Computed diffusion-weighted MR imaging may improve tumor detection. Radiology 2011; 261:573–581.
12. Gatidis S, Schmidt H, Martirosian P, Nikolaou K, Schwenzer NF. Apparent diffusion coefficient-dependent voxelwise computed diffusion-weighted imaging: an approach for improving SNR and reducing T_2 shine-through effects. J Magn Reson Imaging 2016; 43: 824–832.
13. Vural M, Ertaş G, Onay A, et al. Conspicuity of peripheral zone prostate cancer on computed diffusion-weighted imaging: comparison of $cDWI_{1500}$, $cDWI_{2000}$, and $cDWI_{3000}$. Biomed Res Int 2014; 2014:768291.
14. Shimizu H, Isoda H, Fujimoto K, et al. Comparison of acquired diffusion weighted imaging and computed diffusion weighted imaging for detection of hepatic metastases. Eur J Radiol 2013; 82:453–458.
15. Waseda Y, Yoshida S, Takahara T, et al. Utility of computed diffusion-weighted MRI for predicting aggressiveness of prostate cancer. J Magn Reson Imaging 2017; 46: 490–496.
16. Subhawong TK, Jacobs MA, Fayad LM. Diffusion-weighted MR imaging for characterizing musculoskeletal lesions. Radiographics 2014; 34:1163–1177.
17. Inoue C, Fujii S, Kaneda S, et al. Apparent diffusion coefficient (ADC) measurement in endometrial carcinoma: effect of region of interest methods on ADC values. J Magn Reson Imaging 2014; 40:157–161.
18. Heverhagen JT. Noise measurement and estimation in MR imaging experiments. Radiology 2007; 245:638–639.
19. Takayama Y, Nishie A, Asayama Y, et al. Optimization and clinical feasibility of free-breathing diffusion-weighted imaging of the liver: comparison with respiratory-triggered diffusion-weighted imaging. Magn Reson Med Sci 2015; 14:123–132.
20. Yamashita K, Yoshiura T, Hiwatashi A, et al. High-resolution three-dimensional diffusion-weighted imaging of middle ear cholesteatoma at 3.0 T MRI: usefulness of 3D turbo field-echo with diffusion-sensitized driven-equilibrium preparation (TFE-DSDE) compared to single-shot echo-planar imaging. Eur J Radiol 2013; 82:e471–475.
21. Hori M, Irie R, Suzuki M, Aoki S. Teaching neuroimages: obscured cerebral infarction on MRI. Clin Neuroradiol 2017; 27:519–520.
22. Andica C, Hori M, Kamiya K, et al. Spatial restriction within intracranial epidermoid cysts observed using short diffusion-time diffusion-weighted imaging. Magn Reson Med Sci 2018; 17:269–272.